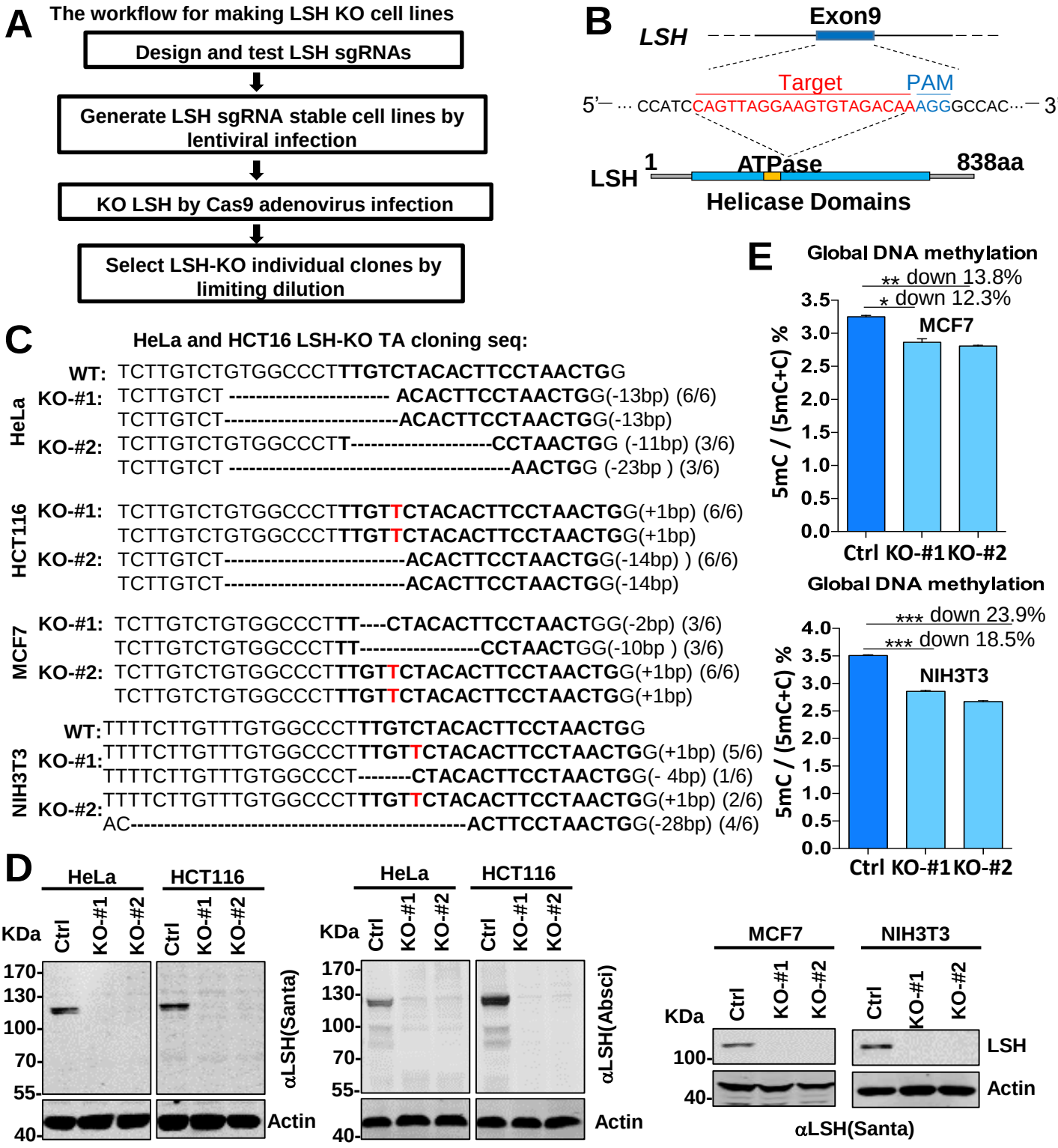

Figure S1. Related to Figure 1. Verification of LSH knockout cell lines generated by CRISPR/Cas9. **A)** The workflow for generating LSH KO cell lines. **B)** Diagram illustrating the guide RNA sequence and position in LSH gene. **C)** Summary of TA cloning sequencing results for each KO cell lines. The numbers of sequenced clones were also indicated. Note the selected LSH guide RNA targeting sequence is completely conserved between human and mouse genome. **D)** Western blotting results showing the loss of LSH proteins in selected KO cell lines. αLSH (Santa) is a mouse monoclonal antibody raised against LSH amino acids 1-240 and αLSH (Absci) is a rabbit antibody raised against LSH amino acids 719-838. **E)** Global levels of DNA methylation for control and LSH KO MCF and NIH3T3 cells determined by quantitative HPLC. *, P<0.05; **, P<0.005; ***, P<0.0005.

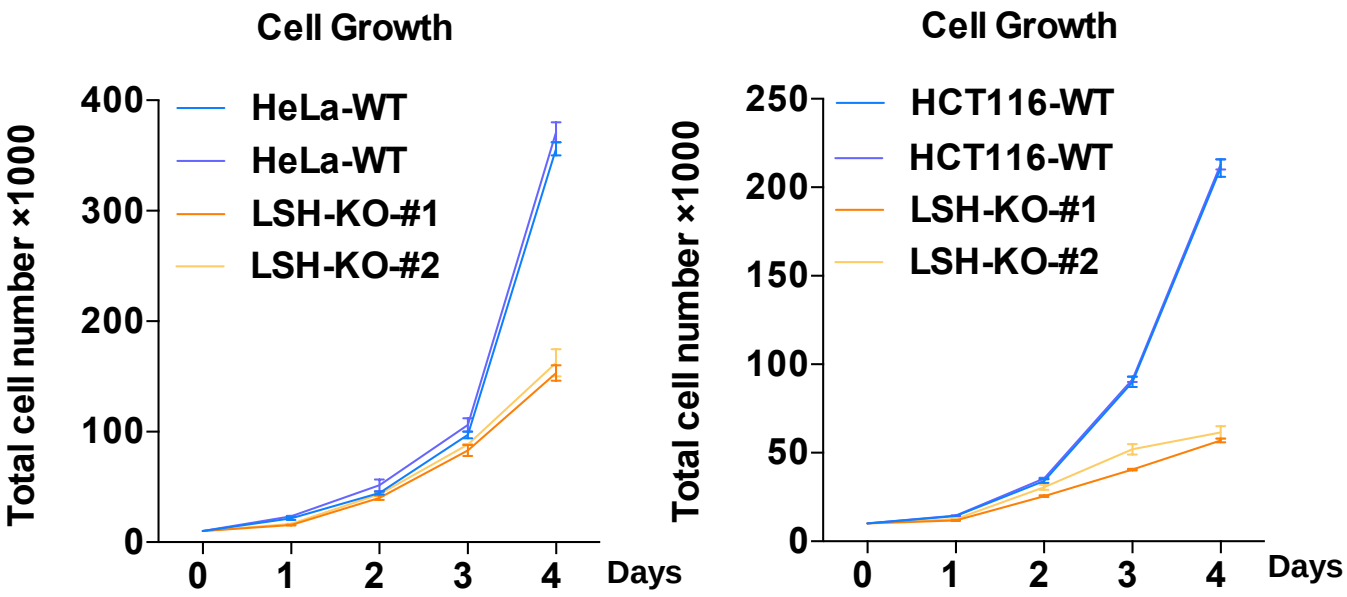

Figure S2. Related to Figure 1. LSH knockout cell lines show reduced cell proliferation. A total number of 10,000 cells for both control parental and LSH KO cells were seeded in triplicate wells in a 6-well plate. The cells were cultured for indicated days and counted. Experiments were repeated at least three times with consistent results. Data are shown as the mean ± s.d.

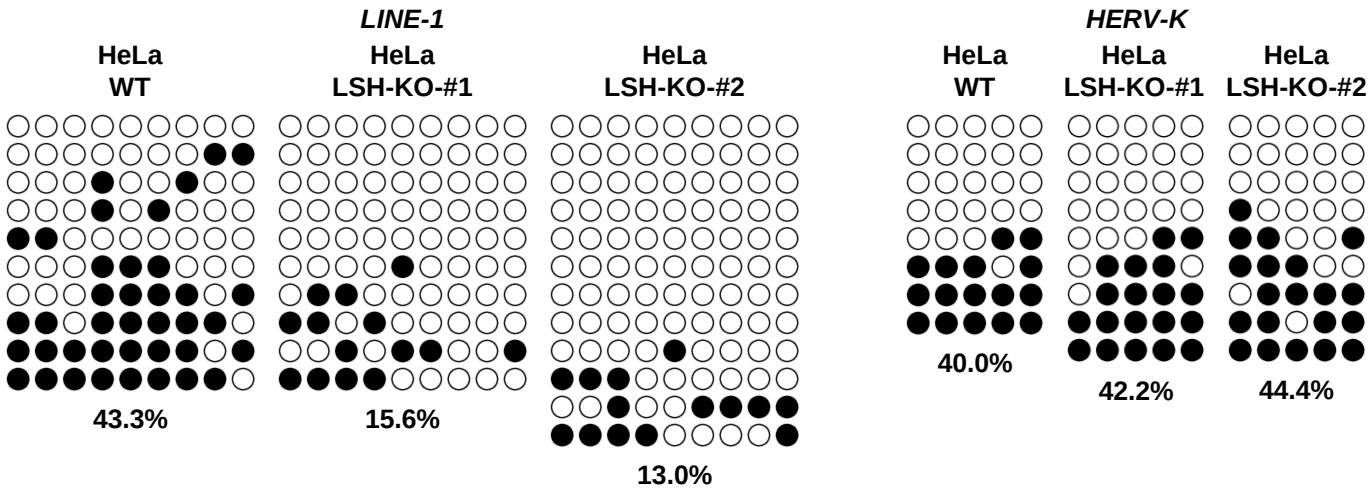

Figure S3. Related to Figure 1. LSH knockout results in substantial reduction of DNA methylation in *LINE-1* sequences. Genomic DNA was prepared from control and LSH knockout HeLa cells respectively and subjected to bisulfite sequencing for both *LINE-1* and *HERV-K* elements as described in Materials and Methods. Note that loss of LSH1 resulted in substantial reduction of the levels of 5-mC in *LINE-1* but not in HERV-K elements.

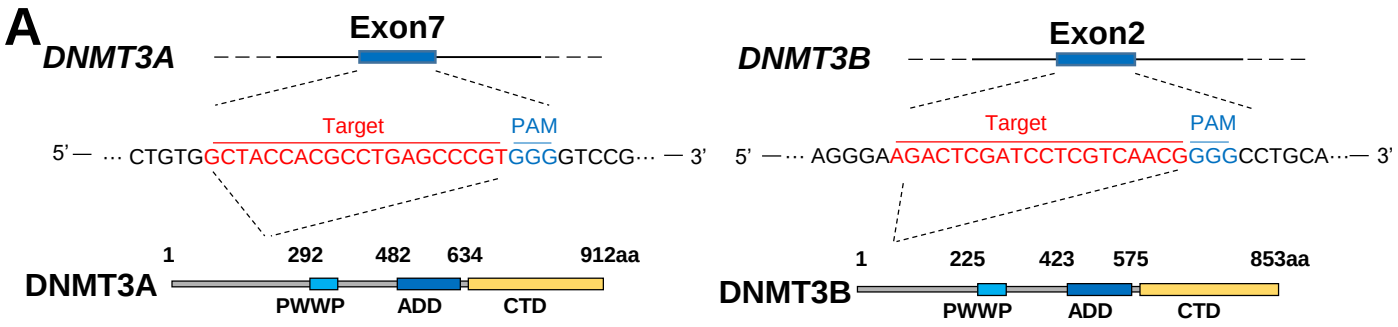

B **HeLa DNMT3A/DNMT3B-DKO TA cloning seq:**

***#1-DKO-DNMT3A* TA cloning seq:**

WT: TGTG**GCTACCACGCCTGAGCCCGT**GGGG
DKO: TGTG**GCTACCACGCCTGAGCCACAGTGGCGT**GGGG (+7bp) (2/6)
TGTG**GCTACCACGCCTGAGCCCCGT**GGGG (+1bp) (4/6)

***#1-DNMT3B* TA cloning seq:**

WT: A**AGACTCGATCCTCGTCAACG**GGGC//TCCGCACCCCGG
DKO: A**AGACTCGATCCT----------**CCGG (-64bp) (1/6)
A**AGACTCGATCCTCGTCAAACG**GGGC//TCCGCACCCCGG (+1bp) (5/6)

***#2-DKO-DNMT3A* TA cloning seq:**

WT: TGTG**GCTACCACGCCTGAGCCCGT**GGGG
DKO: TGTG**GCTACCACGCCTGAGCTCG--**GGGG(-1bp) (3/6)
TGTG**GCTACCACGCCTGAGCC--GT**GGGG(+1bp) (3/6)

***#2-DNMT3B* TA cloning seq:**

WT: A**AGACTCGATCCTCGTCAACG**GGGCCTGC
DKO: A**AGACTCGATCCTCGTCAAACG**GGGCCTGC(+1bp) (4/6)
A**AGACTCGATCCTCG----------**CCTGC (- 9bp) (2/6)

C **HeLa LSH/DNMT3A/DNMT3B-TKO TA cloning seq:**

***LSH* TA cloning seq:**

WT: TCTTGTCTGTGGCCCT**TTGTCTACACTTCCTAACTG**GATGG
TKO-#1: TCTTGTCTGT**----------TCCTAACTG**GATGG(-17bp) (3/8)
TCTTGTCTGTGGCCCT**T----------CCTAACTG**GATGG(-11bp) (5/8)
TKO-#2: TCTTGTCTGTGGCCCT**TTGTTCTACACTTCCTAACTG**GATGG(+1bp) (6/8)
TCTTGTCTGTGGCCCT**TTGT----------AACTG**GATGG(-11bp) (2/8)

Figure S4. Related to Figure 2. Verification of DNMT3A/3B-DKO and DNMT3A/3B/LSH-TKO cell lines by sequencing. **A)** Diagram illustrating the guide RNA sequence and position for disruption of DNMT3A and DNMT3B genes by CRISPR/Cas9 . **B,C)** Summary of TA cloning sequencing results for corresponding KO cell lines. Also indicated are numbers of clones sequenced.

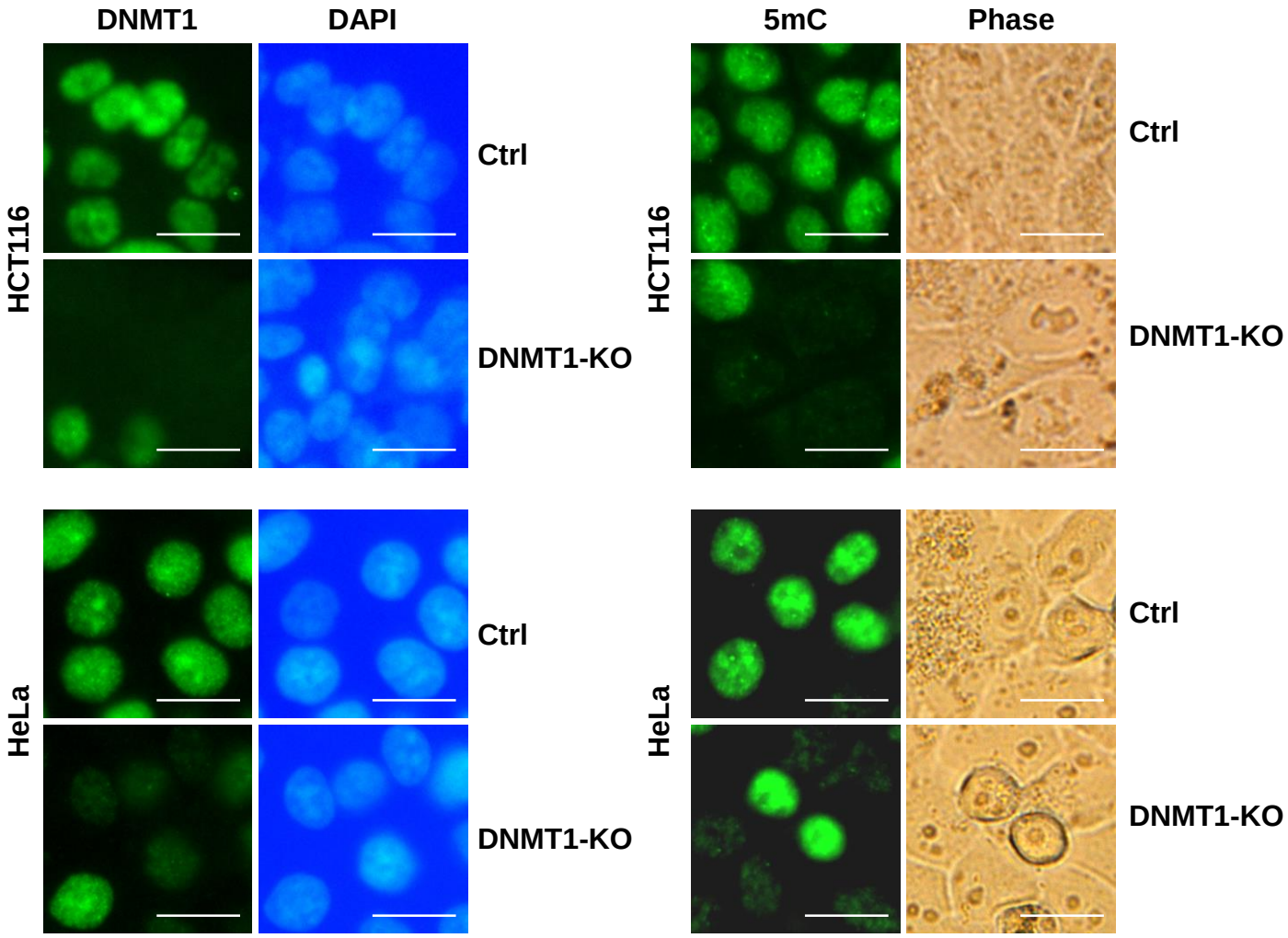

Figure S5. Related to Figure 2. DNMT1 knockout caused global DNA demethylation in HCT116 and HeLa cells. Representative immunostaining images showing that global DNA methylation level was dramatically reduced in HCT116 and HeLa cells in which DNMT1 was transiently knocked out by CRISPR/Cas9 technology. The remaining cells positive for either DNMT1 or 5-mC staining were cells escaped from DNMT1 knockout and served as control. The 5mC positive cells in DNMT1-KO images represent cells escaped from DNMT1 knockout. Scale bar, 20μm.

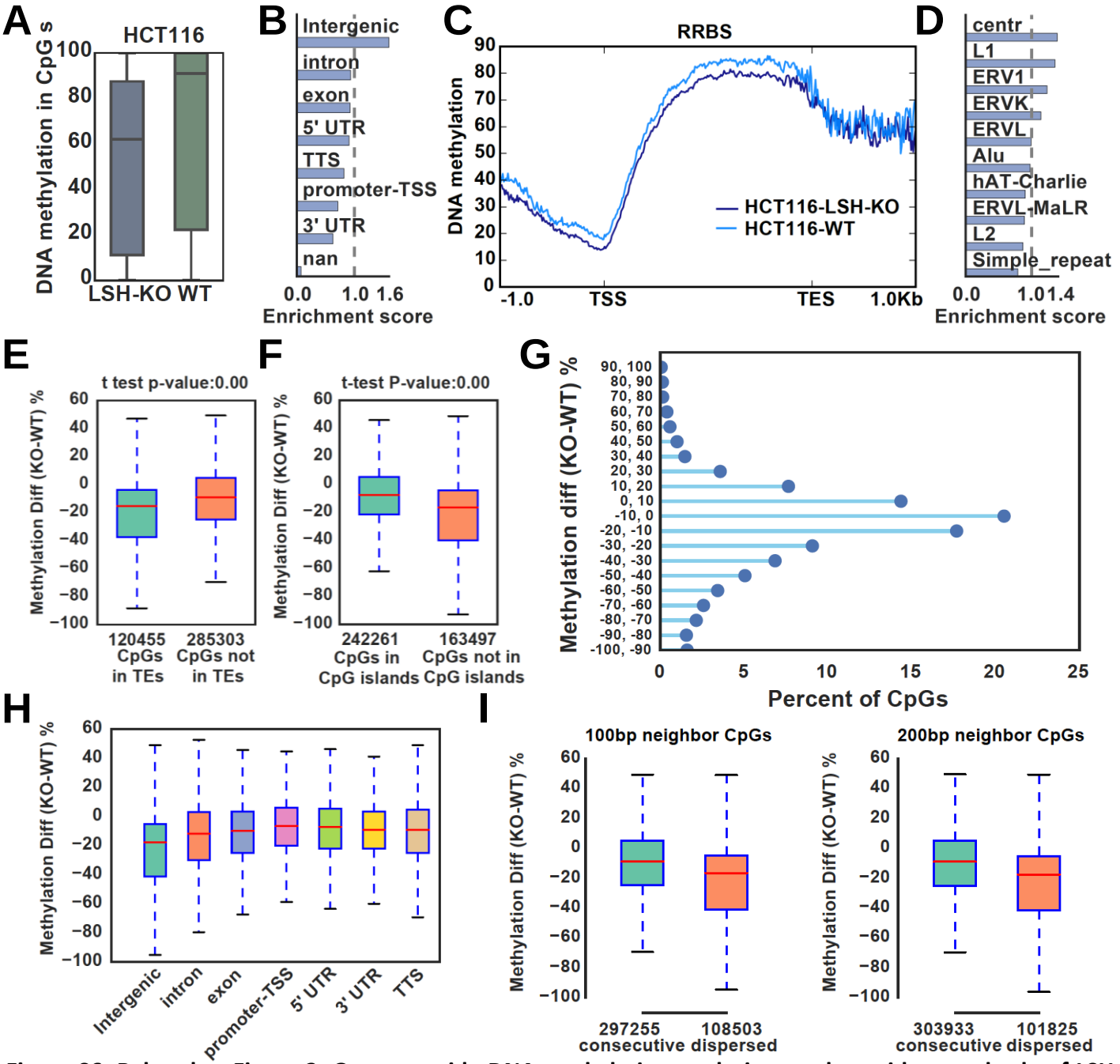

Figure S6. Related to Figure 3. Genome-wide DNA methylation analysis reveals a widespread role of LSH in DNA methylation. **A)** Global distribution and mean levels of CpG methylation in control HCT116 and LSH KO cells. The line represents the median levels of distribution. **B)** Genomic distribution of CpGs with highly reduced methylation (WT-KO>30%, 276,513 CpGs). **C)** Average CpG methylation levels for all genes and flanking 1kb regions in control HeLa and LSH KO cells. TSS, transcription start site.; TES, transcription end site. **D)** Genomic distribution of CpGs with highly reduced methylation (WT-KO>30%) that were mapped to transposon elements. **E)** Comparison of methylation differences between control and LSH-KO cells in and not in transposable elements regions. **F)** Comparison of methylation differences between control and LSH-KO cells in and not in CpG islands. **G)** All CpG sites were plotted according to the difference in levels of CpG methylation between control and LSH-KO cells. The Y axes represents distribution of CpG sites with DNA methylation in KO cells that were reduced from 0 to 100% or increased from 0 to 100% as compared to control. X axes represents the percentage of CpG sites in each category with a total of 100%. **H)** Distribution of CpG methylation changes at different genomic regions. **I)** Distribution of CpG methylation changes at consecutive CpG sites and dispersed sites. Consecutive CpGs were defined as more than one CpG located in 100 bp (left) and 200 bp (right).

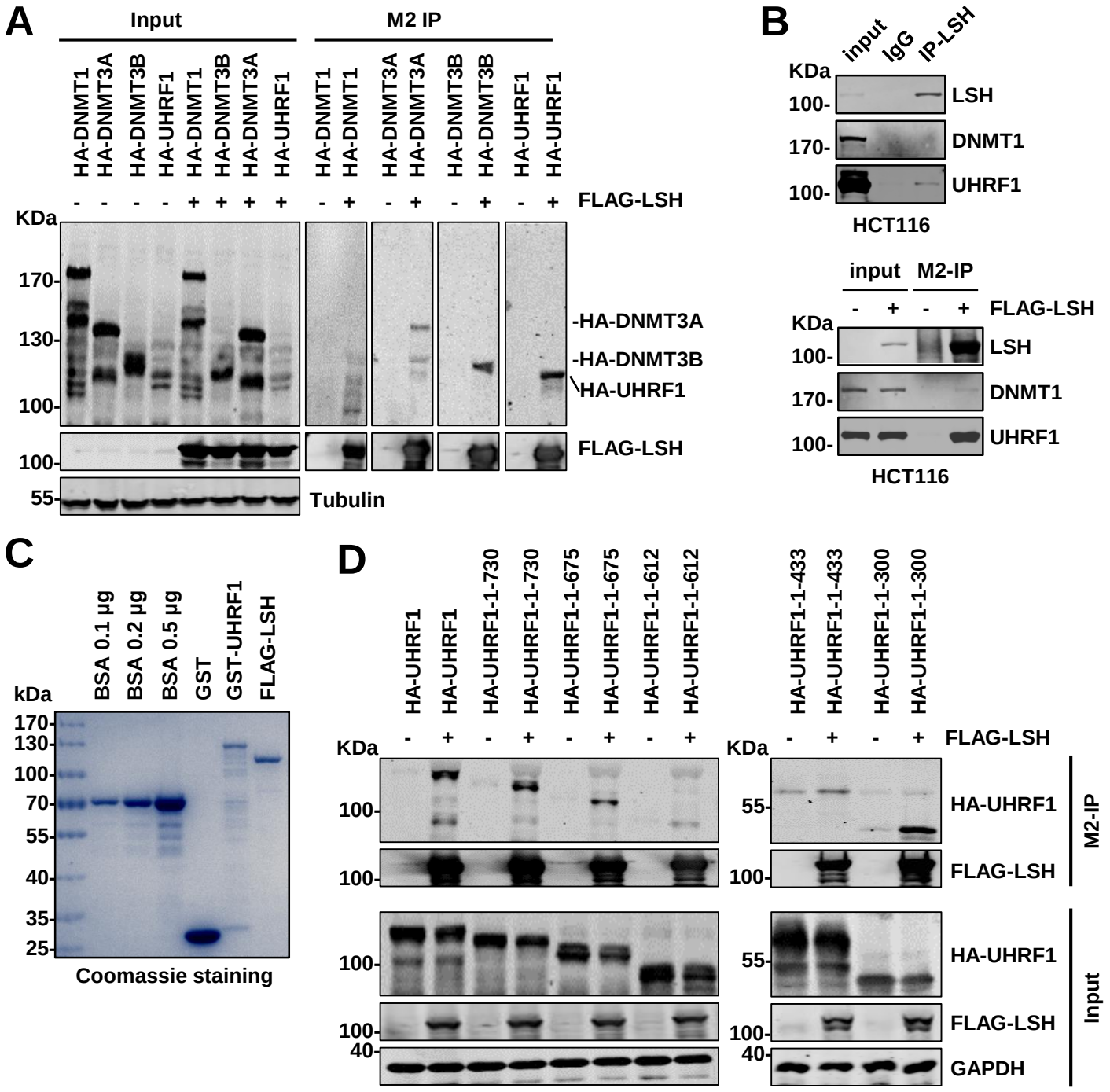

Figure S7. Related to Figure 5. Characterization of the interaction between LSH and DNMTs and UHRF1. **A)** Western blotting showing that ectopically expressed LSH co-immunoprecipitated with co-expressed DNMT3A, DNMT3B and UHRF1 but not DNMT1 in 293T cells. **B)** Western blotting showing that endogenous LSH co-immunoprecipitated with UHRF1 but not DNMT1 and ectopically overexpressed LSH co-immunoprecipitated robustly with UHRF1 but slightly with DNMT1 in HCT116 cells. **C)** Coomassie blue staining showing purified recombinant FLAG-LSH, GST and GST-UHRF1 that were used for pulldown assay in Figure 5E. **D)** Co-IP assay showing the interaction between LSH and various UHRF1 deletion mutants.

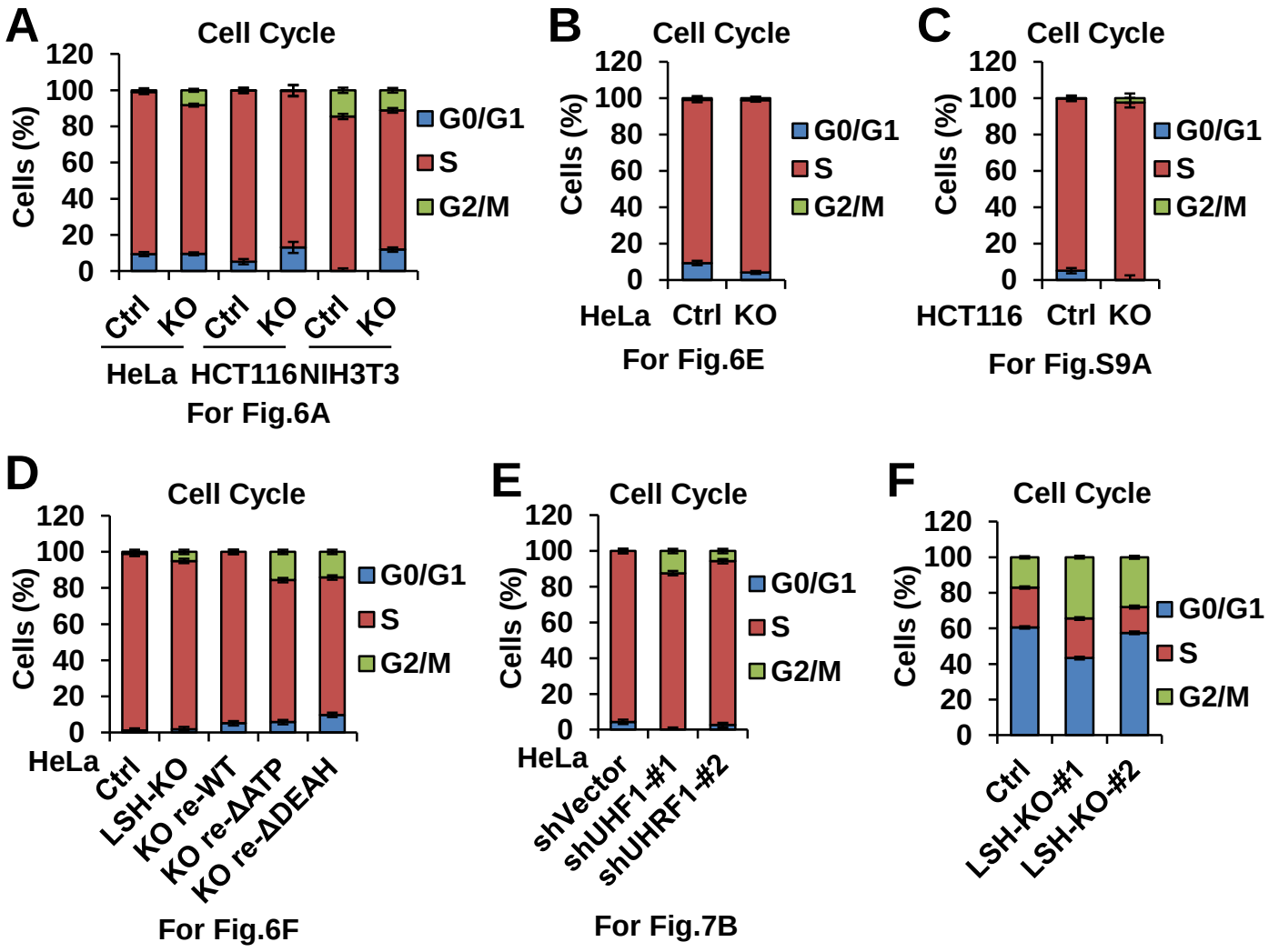

Figure S8. Related to Figure 6. Cell cycle analysis by FACS. A) Control and LSH-KO HeLa, HCT116 and NIH3T3 cells synchronized to S phase in experiments in Figure 6A were analyzed by FACS to determine the cell cycle status. Note after synchronization protocol more than 80% cells were characteristic of S phase. **B)** Cells for experiments in Figure 6E were analyzed by FACS to determine the cell cycle status. Note after synchronization protocol more than 85% cells were in S phase. **C)** Cells for experiments in Figure S9A were analyzed by FACS to determine the cell cycle status. Note after synchronization protocol more than 90% cells were in S phase. **D)** Cells for experiments in Figure 6F were analyzed by FACS to determine the cell cycle status. Note after synchronization protocol more than 75% cells were in S phase. **E)** Cells for experiments in Figure 7B were analyzed by FACS to determine the cell cycle status. Note after synchronization protocol more than 85% cells were in S phase. **F)** Unsynchronized control and LSH-KO HeLa Cells were analyzed by FACS to determine the cell cycle status.

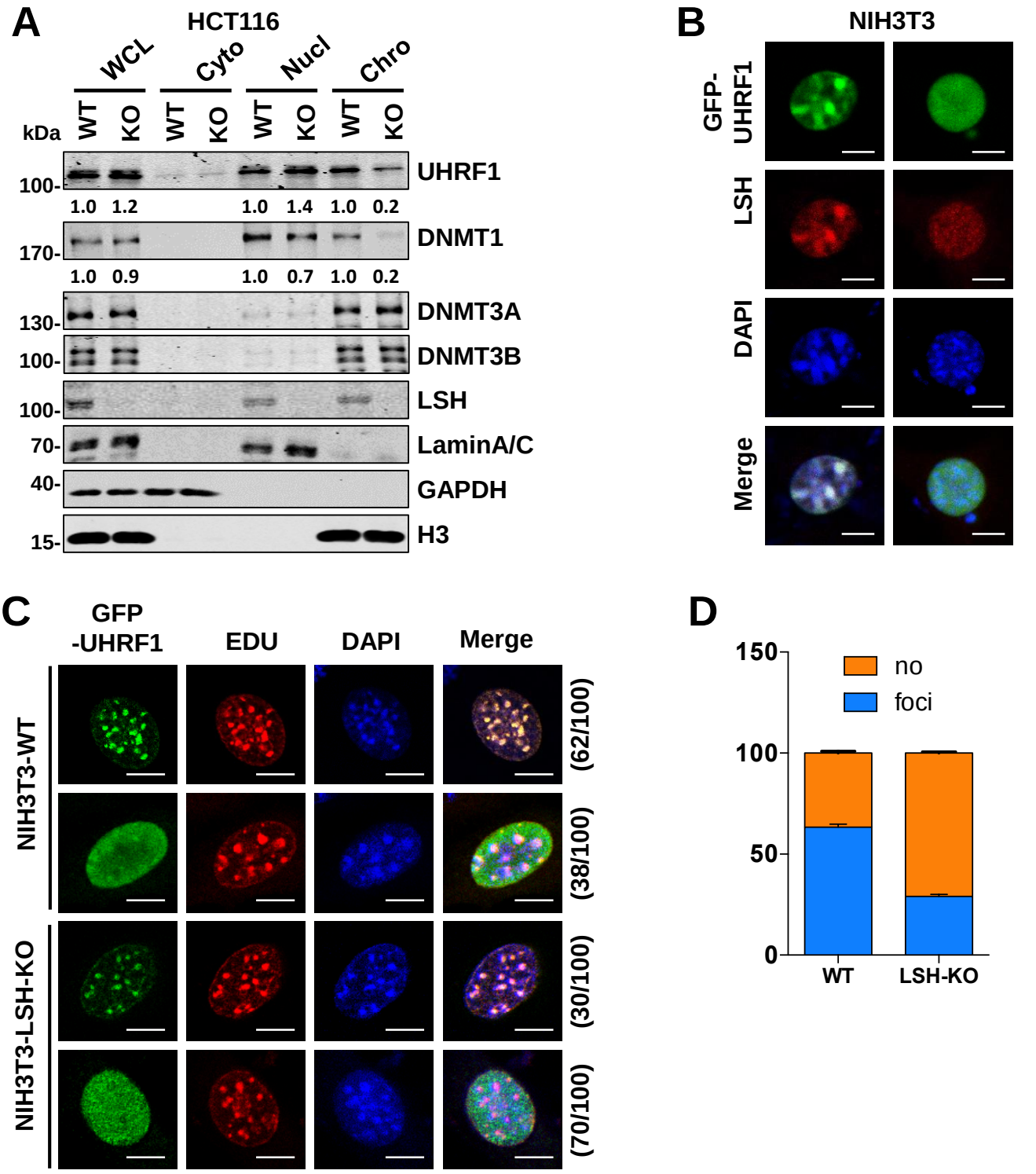

Figure S9. Related to Figure 6. LSH promotes UHRF1 and DNMT1 chromatin association in S phase of cell cycle. A) Cellular fractionation followed by Western blot analysis showing LSH knockout reduced chromatin-associated UHRF1 and DNMT1 in S phase of HCT116 cells. The cells were synchronized to S phase by using aphidicolin treatment followed by releasing cells into fresh medium without aphidicolin for 2 h. **B)** GFP-UHRF1 colocalized with LSH and heterochromatin DAPI foci in NIH3T3 cells. Scale bar, 10 μm. **C)** LSH knockout substantially reduced the number of mid-to-late S phase cells with pericentromeric heterochromatin colocalized GFP-UHRF1. Scale bar, 10 μm. **D)** Quantitative results of per data in C).